Catal Lett (2016) 146:2324–2329
DOI 10.1007/s10562-016-1862-y

Effect of Graphitic Carbon Nitride on the Electronic and Catalytic Properties of Ru Nanoparticles for Ammonia Synthesis

Zhanwei Ma[1,2] · Shengli Zhao[1,2] · Xumao Xiong[1] · Bin Hu[1] · Chengli Song[1]

Received: 18 July 2016 / Accepted: 7 September 2016 / Published online: 24 September 2016

Abstract Graphitic carbon nitrides were employed to prepare the Ruthenium-based ammonia synthesis catalysts by thermal decomposition of $Ru_3(CO)_{12}$ under N_2 or H_2 atmosphere. Different pretreatment atmospheres significantly affected the interaction between Ru nanoparticles and the graphitic carbon nitride. The strong metal support interaction enhanced the electronic density transfer from rich-electron π-plane of the support to the Ru nanoparticles. And it further caused the upshift of d-band center of Ru nanoparticles. The upshift of d-band center improved the ability of surface to bond to N_2, and consequently the ammonia synthesis activity was enhanced.

Graphical Abstract Electron-rich and graphitic carbon nitride enhanced the electron density of Ru nanoparticles. And that caused the upshift of d-band center of Ru nanoparticles. This upshift of d-band center improved the ability of surface to bond to N_2, and consequently the ammonia synthesis activity was enhanced.

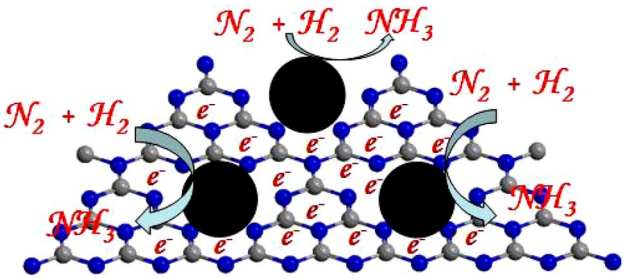

Keywords Graphitic carbon nitride · Ammonia synthesis · d-Band model · Ru nanoparticls · Strong metal support interaction

1 Introduction

Ammonia catalytic synthesis is one of the most important catalytic processes in chemical industry. As such, a large number of studies have been focused on developing effective catalysts to access the ammonia and understanding the mechanism. It is well-known that the dissociative adsorption of N_2 is the rate-determining step of ammonia synthesis [1]. And N_2 dissociation always is related to the geometric structure (the so-called B_5-type sites) and the electronic properties of Ru nanoparticles. Following the previous studies, the most active sites (B_5-type sites) are preferentially formed on small particles (1.8–3.5 nm) [2]. Electronically, the strong metal support interaction (SMSI) promotes the injection of electrons to the antibonding π^*-orbital of N_2 molecule so that the N≡N bond could be easier weakened and resulted in the cleavage [3]. To date, none but graphite carbon-supported Ru catalysts have been used for ammonia synthesis industry. In the case of Ru/C catalyst system, it

Electronic supplementary material The online version of this article (doi:10.1007/s10562-016-1862-y) contains supplementary material, which is available to authorized users.

✉ Bin Hu
Hcom@licp.cas.cn

✉ Chengli Song
songchl@licp.cas.cn

[1] State Key Laboratory for Oxo Synthesis and Selective Oxidation, Lanzhou Institute of Chemical Physics, Chinese Academy of Sciences, Lanzhou 730000, China

[2] University of Chinese Academy of Sciences, Beijing 100049, China

has been found that the graphitization of carbon materials altered the electronic conductivity and then enhanced the catalytic activity [4]. In addition, the carbon-supported Ru catalysts without the promoters of alkali or alkaline earth metal oxide are completely inactive [5, 6]. Nitrogen-doped carbon nanotubes [7], however, exhibited considerable activity without promoters due to the electron-donating nitrogen and the graphitization of carbon nanotubes. Recently, the electron-rich electrides $[Ca_{24}Al_{28}O_{64}]^{4+}(e^-)_4$ [8] and Y_5Si_3 [9] with strong electron-donating ability were introduced as supports for ammonia synthesis, which obviously enhanced N_2 molecule dissociation and reduced the activation energy of the reaction. Inspired by these successes, the new support containing electron-donating nitrogen, graphitization and electron-rich carbon material may be promised to become an alternative candidate.

Graphitic carbon nitride (g-C_3N_4), as an analogue of graphite, has electron-donating nitrogen which could be tunable and alter its chemical and physical properties such as surface basicity, polarity and conductivity [10]. The nitrogen species in g-C_3N_4 play roles in dispersing and stabilizing metal nanoparticles [11]. The recent works of hydrogenation of phenol [12] and quinoline [13] on Pd@g-C_3N_4 indicated the rich-electron π-plane enhanced the transfer of electron density from the g-C_3N_4 support to the metallic Pd and thereby accelerated the hydrogenation reaction. Furthermore, the heterojunction effect leads to the electron transfer from the g-C_3N_4 semiconductor to noble metals (such as Ru, Pd, Ag) [14]. This transfer of electron density led to the d-band center of metal nanoparticles being upshifted toward the Fermi level [15]. In the light of the d-band model [16–18], the upshift or downshift of the d-band center determines the level of difficulty in activation of N_2 molecule on Ru nanoparticles. In this work, highly dispersed Ru nanoparticles were synthesised and their catalytic behaviours on the rich-electron π-plane of the g-C_3N_4 support were investigated.

2 Experimental

2.1 Catalyst Preparation

The g-C_3N_4 was prepared by polymorization of melamine molecules under high temperature. In detail, melamine was heated at 873 K for 2 h under air condition with a ramp rate of 2.3 K/min for the heating process. The obtained orange product was the g-C_3N_4 powder.

The orange g-C_3N_4 powders were stirred with a solution of ruthenium carbonyl ($Ru_3(CO)_{12}$) in THF at room temperature for 12 h in a rotary evaporator. And then the solvent was removed under reduced pressure at 303 K. The gray powders were calcined at 553 K for 3 h under hydrogen atmosphere, followed by cooling in H_2 atmosphere to room temperature to obtain the final Ru-H/g-C_3N_4 catalyst (Fig. S1). The support H-g-C_3N_4 (without the presence of Ru nanoparticles) was obtained under the same pretreatment condition of Ru-H/g-C_3N_4. For comparison, γ-Al_2O_3, MgO, Graphite, graphitic activated carbon (g-AC) and CeO_2 supported Ru catalysts were also synthesised at a Ru content of 4% by the same way **(**Supporting Information**)**. Only the Ru-N/g-C_3N_4 catalyst was prepared under N_2 atmosphere. The Ru loadings of Ru-N/g-C_3N_4 and Ru-H/g-C_3N_4 were determined by XRF measurements, 3.94 and 3.87%, respectively.

2.2 Catalyst Characterisation

The crystalline structure of the samples was analyzed by X-ray powder diffraction (XRD) (X′pert, PANalytical, Dutch) using Cu Kα radiation (λ = 1.54050 Å). Crystallite size of the support was calculated by the Scherrer equation. Transmission electron microscope (TEM) experiments were conducted in a JEM-2010 TEM with an accelerating voltage of 200 KV. The element compositions were detected by X-ray photoelectron spectrometer (XPS, ESCALAB 250Xi). The FT-IR spectra of samples were recorded on a NEXUS 670 FT-IR spectrometer with KBr pellets prepared by manual grinding.

2.3 Catalyst Evaluation

In ammonia synthesis reaction, 0.2 g catalyst was used for each experiment. And then the catalyst diluted with quartz sand to 2 ml [stainless steel microreactor (φ = 6 mm)]. The catalyst was stabilized under different temperature for 1 h (reaction conditions: 3 MPa, 5000 h^{-1}, the purity of nitrogen and hydrogen: 99.999%, $H_2/N_2 = 3$), then the data were collected when the ammonia synthesis reaction had reached a steady state. The ammonia synthesis rates in the effluent were determined by a chemical titration method with a known amount of H_2SO_4 (Congo red as indicator) [19].

3 Results and Discussion

Firstly, the catalytic activities for ammonia synthesis over various 4% Ru-loaded catalysts were investigated (Fig. S2). Compared with the Ru-H/g-C_3N_4 catalyst, the Ru-N/g-C_3N_4 catalyst had much less activity. Under the same reaction conditions, the catalysts Ru/g-AC and Ru/Graphite were nearly inactive. Then, the Ru-N/g-C_3N_4 and Ru-H/g-C_3N_4 catalysts were used to continuously produce NH_3 for 44 h, the Ru-N/g-C_3N_4 catalyst still kept the number of its activity at a low level. These results indicated that the thermal decomposition of the $Ru_3(CO)_{12}$ precursor on g-C_3N_4

under different atmospheres such as H_2 and N_2 significantly affected the activity of the resulting catalysts.

The results motivated us to further consider the structure properties of the Ru-N/g-C_3N_4 and Ru-H/g-C_3N_4 catalysts. The graphitic packing structure of carbon nitride was proven by powder X-ray diffraction (Fig. 1). The XRD patterns show the characteristic peak of (002) packing of graphitic carbon nitride at 27.5° and the corresponding lattice spacing is 0.32 nm. The diffraction peaks at 38.3°, 42.2°, 44.0°, 58.3°, 69.4°, 78.4°, 84.7° and 85.9° can be ascribed to the metallic Ru (Hexagonal, JCPDS: 03-065-7646, Fig. 1 inset). The average size of the crystallites was calculated to be ~5.5 nm (Ru-H/g-C_3N_4) and ~6.2 nm (Ru-N/g-C_3N_4) by Scherrer's formula. The morphologies of the Ru-H/g-C_3N_4 and Ru-N/g-C_3N_4 catalysts were also investigated by TEM (Fig. 2 and Fig. S3). For the Ru-H/g-C_3N_4 catalyst, it can be noted that the Ru nanoparticles were well dispersed on g-C_3N_4 in H_2 atmosphere. The HRTEM images revealed the well-dispersed Ru particles with a mean size of 3.2 nm (Fig. 2d), which was slightly smaller than the value predicted by XRD. Furthermore, the lattice spacing of 0.214 nm measured out in the HRTEM image (Fig. 2b) was well indexed to the (002) plane of Ru nanoparticles. The HAADF-STEM investigation (Fig. 2e, f) showed the presence of Ru nanoparticles dispersed on the samples, clearly seen due to the atomic number (Z) contrast. A brighter area in the elemental map indicated a higher concentration of the corresponding element in that area. Different elements were shown in different colors to identify their positions within the catalysts. Obviously, the C and N distributions were uniform and continuous. In contrast, the distribution of Ru was discrete, indicating the Ru nanoparticles were well dispersed on the surface of g-C_3N_4. However, the Ru nanoparticles with a mean size of 4.8 nm were partially aggregated (Fig. S3) in the Ru-N/g-C_3N_4

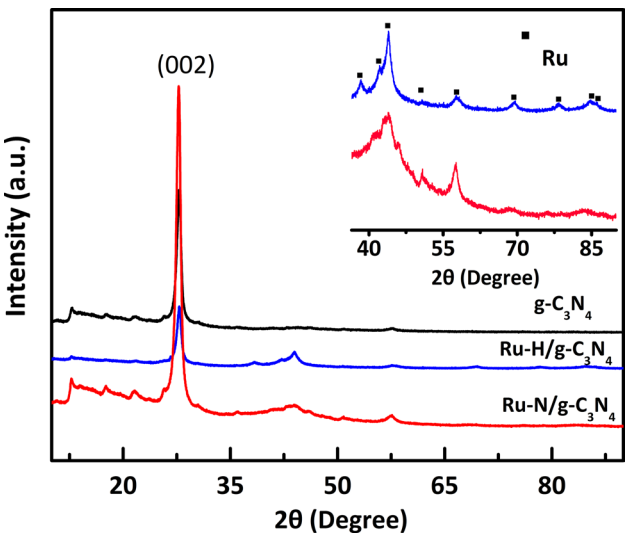

Fig. 1 XRD patterns of the g-C_3N_4, Ru-H/g-C_3N_4 and Ru-N/g-C_3N_4

catalyst. And the distribution range of Ru nanoparticles was even wider. Dong et al [20] have confirmed that the N_2 molecular can adsorbe on the surface nitrogen vacancies of g-C_3N_4 and Pd particles can be selectively deposited onto the nitrogen vacancies of g-C_3N_4. Thus, the larger size and partical aggregation of Ru nanoparticles could be ascribed to the N_2 occupying the nitrogen vacancies and further affecting the interaction between Ru nanoparticles and g-C_3N_4. The most active sites (B_5-type sites) are preferentially formed on small particles (1.8–3.5 nm), while previous work [21] revealed that the ammonia synthesis activity increased with the average size of Ru nanoparticles in the range 2–10 nm, and the synergic effect between the large and small nanoparticles played a crucial role. In addition, the recent work [22] showed the different sizes of Ru particles were not the major reason for changing the activity of Ru catalysts.

Inspired by these exciting diversities of the catalysts, XPS spectra were employed to investigate the electron properties of Ru and g-C_3N_4. Figure 3 displays the XPS survey spectra and the corresponding high resolution XPS spectra of the resulting Ru-H/g-C_3N_4 and the Ru-N/g-C_3N_4 catalysts. The peak positions in all of the XPS spectra were calibrated with C 1s at 284.8 eV. The C 1s peak at 284.8 eV derived from carbonaceous impurities. The N 1s peak appearing at 399 eV is assigned to the sp^2-bonded N atoms in triazine rings (C–N=C) [23]. After H_2 pretreatment, the N 1s peak of the support H-g-C_3N_4 did not shift. However, for the Ru-H/g-C_3N_4 catalyst, the binding energy of N 1s shifted +1 eV to the higher position 400 eV and the Ru 3d binding energy shifted −0.8 eV to the lower position 279.6 eV relative to the metallic Ru (280.2 eV). However, the Ru 3d binding energy of the Ru-N/g-C_3N_4 catalyst shifted +0.2 eV to the binding energy 280.4 eV and the N 1s binding energy at 399 eV did not clearly shift. These results implied that the Ru nanoparticles dispersed on the different sites of the g-C_3N_4 structure under different atmospheres. As reported previously [20], Ru nanoparticles can be selectively deposited onto the nitrogen vacancies of g-C_3N_4 during H_2 pretreatment. Under N_2 atmosphere, however, N_2 occupying the nitrogen vacancies caused the Ru nanoparticles located other sites. These different sites induced the different strength of interaction generated between the Ru nanoparticles and g-C_3N_4 support. The chemical shift of Ru 3d5/2 core level suggested the d-band center of Ru nanoparticles is shifted [24–26]. Thus, the negative chemical shift indicated an upward shift of d-band center, contrarily, the positive chemical shift suggested a downward shift. According to the Hammer–Nørskov model [16, 18], such upshifted d-band center leads to stronger interaction of the d-band with the high-lying antibonding of N_2 molecule, causing easier activation of N_2 molecule by enhancement of its antibonding π^* orbital and/or by depleting the π and 5σ bonding orbitals [27]. Therefore, the negative chemical shift is more advantageous than

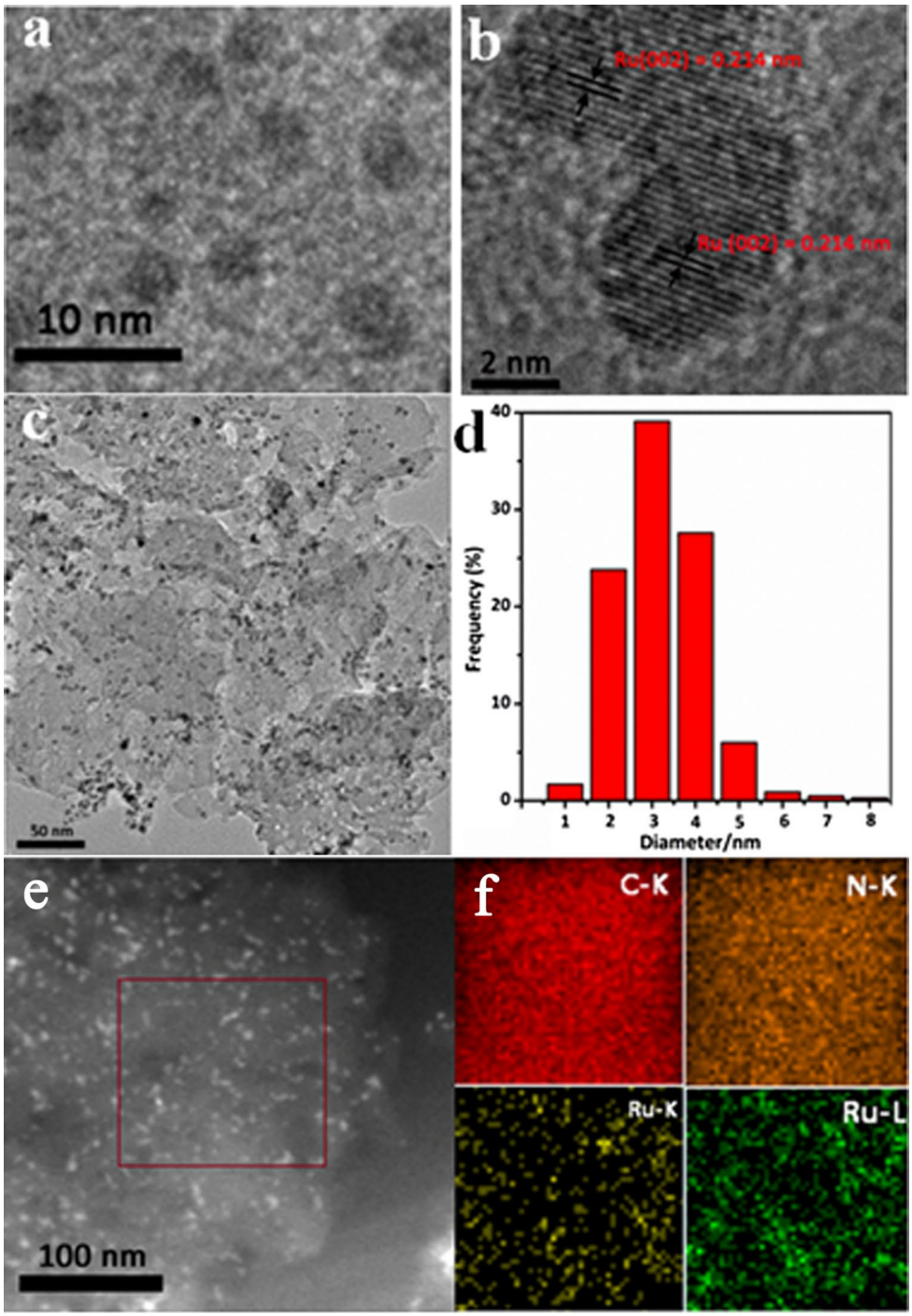

Fig. 2 Typical TEM and STEM-HAADF images **a–c, e** of Ru-H/g-C_3N_4. **d** The particle size distribution of Ru nanoparticles. **f** The elemental mapping of C, N and Ru in Ru-H/g-C_3N_4

the positive chemical shift to activate the N_2 molecule, so that the activity of ammonia synthesis on the Ru-H/g-C_3N_4 catalyst was higher than that on the Ru-N/g-C_3N_4 catalyst. It has been reported [11] that pyridinic N species can be partially reduced to graphitic N species under H_2 atmosphere. Simultaneously, graphitic N species can stabilize the metal particles by the strong interaction. Therefore, the relative percentages of pyridinic N and graphitic N species have been obtained from the area ratio of the peaks (Fig. S4). In this way, the amount of pyridinic N and graphitic N species were 58.1 and 27.8% in the Ru-N/g-C_3N_4 catalyst, respectively. In the Ru-H/g-C_3N_4 catalyst, the amount of pyridinic N species decreased to 53.7% and that of graphitic N species increased to 32%. These combining with the TEM results indicated the graphitic N species can stabilize the Ru nanoparticles.

The structures of the g-C_3N_4, Ru-H/g-C_3N_4 and Ru-N/g-C_3N_4 samples can be further confirmed by FTIR spectroscopy. As shown in Fig. 4, the characteristic IR spectrum of the Ru-N/g-C_3N_4 is similar to that of the g-C_3N_4.

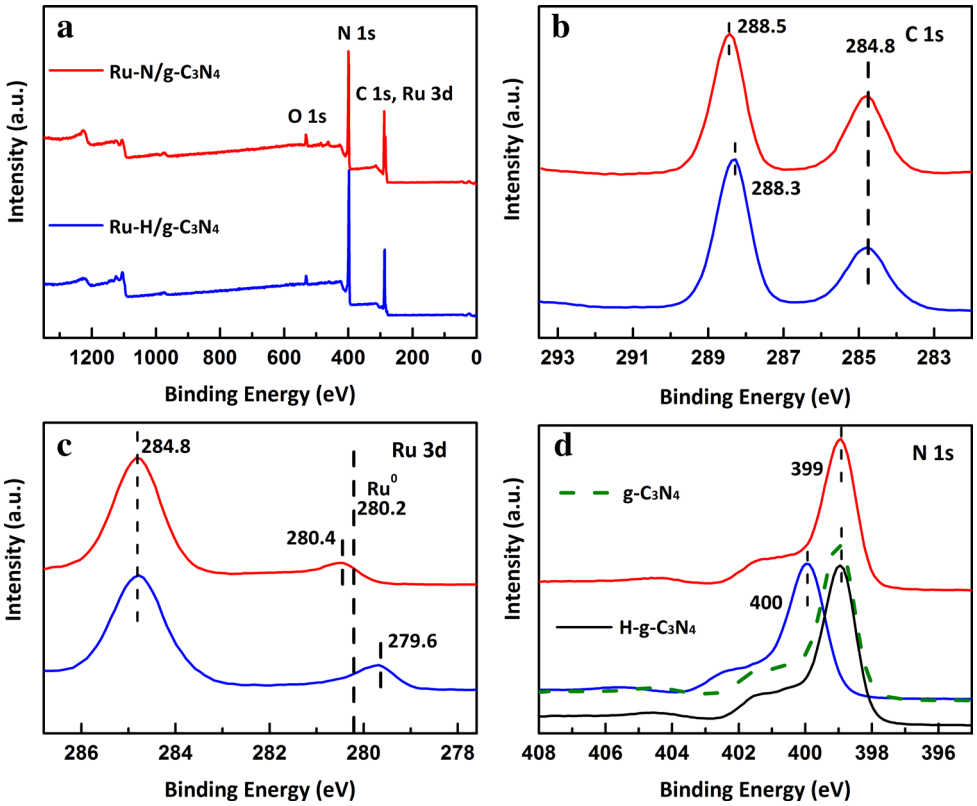

Fig. 3 XPS spectra of the Ru-H/g-C_3N_4 and Ru-N/g-C_3N_4 and the high resolution XPS spectra: C 1s, Ru 3d and N 1s

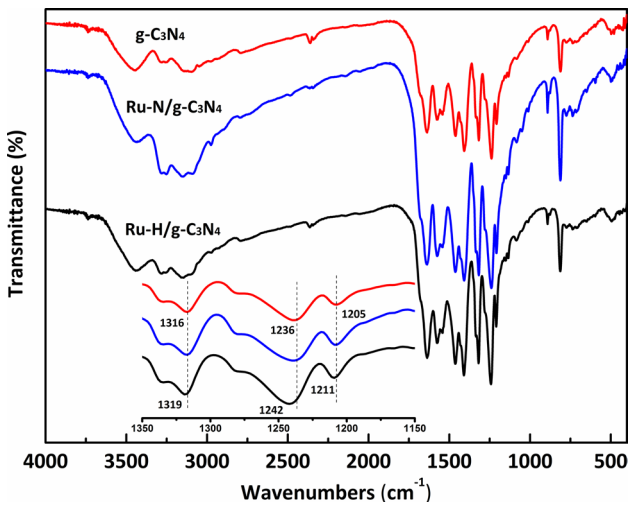

Fig. 4 FTIR spectra of g-C_3N_4, Ru-H/g-C_3N_4 and Ru-N/g-C_3N_4 samples

The broad peak at 3000–3500 cm^{-1} is ascribed to the stretching vibration of N–H and the stretching vibration of O–H of the physically adsorbed water [28]. The peak at 813 cm^{-1} is associated with the characteristic breathing mode of triazine units [29]. The peak at 1636 cm^{-1} and the five strong peaks at 1236, 1205, 1316, 1412 and 1571 cm^{-1} could be assigned to C=N and C–NH–C stretching vibration modes of heterocycles [23, 30]. However, compared with the g-C_3N_4 and Ru-N/g-C_3N_4 samples, the C–N stretching vibration peaks at 1236, 1205, 1316 cm^{-1} shifted to 1242, 1211, 1319 cm^{-1} in the Ru-H/g-C_3N_4 sample, indicating there is the strong interaction between g-C_3N_4 and Ru nanoparticles during the H_2 pretreatment. This result is in accordance with the XPS analysis.

TG-DTA analysis has been carried out to analyze the effect of Ru nanoparticles on the support g-C_3N_4. As shown in Fig. S5, the pure g-C_3N_4 can endure high temperatures and decompose above 600 °C. While the Ru-H/g-C_3N_4 had the clear weight loss at 549 °C, which suggested that there is indeed a strong interaction between Ru nanoparticles and the g-C_3N_4 support, so that it altered the decomposition temperature of the support g-C_3N_4. After the ammonia synthesis reaction, the used Ru-H/g-C_3N_4 catalyst was investigated by FTIR (Fig. S6) and TEM (Fig. S7). The spectrum of the used Ru-H/g-C_3N_4 catalyst was similar to that of the fresh Ru-H/g-C_3N_4 catalyst. It can be obviously observed that Ru nanoparticles were well dispersed on the g-C_3N_4 support. The apparent activation energy of the reaction (Fig. 5a) on the Ru-H/g-C_3N_4 catalyst is 88.5 KJ/mol, which is smaller than Ru-Cs/MgO (100 KJ/mol) and Ba-K-Ru/AC (110–116 KJ/mol) catalysts [19]. The effect of pressure on ammonia synthesis rate was measured from 0.1 to 3 Mpa (Fig. 5a inset). Different kinds of supports were also employed to compare the ammonia synthesis activity (Fig. 5b), such as the acid γ-Al_2O_3, the strong basic MgO, g-AC, graphite and the weak basic CeO_2. It can be observed that Ru/g-AC was

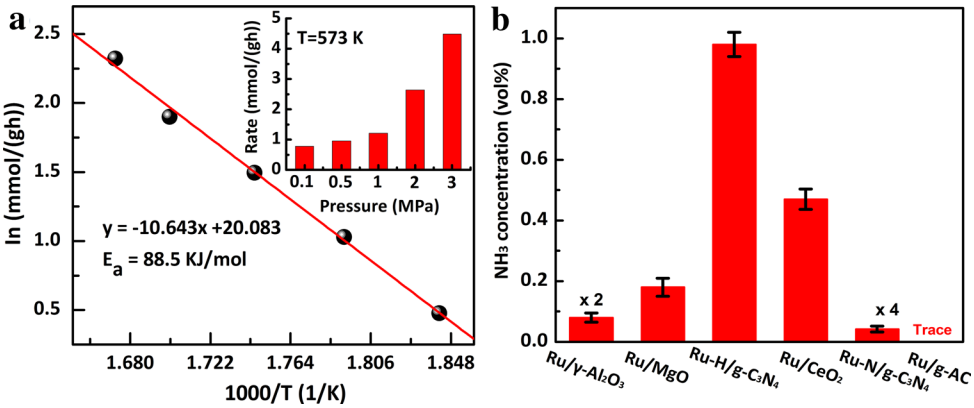

Fig. 5 **a** Apparent activation energies for ammonia synthesis over Ru-H/g-C_3N_4 catalysts under the conditions: 3 Mpa, 5000 h^{-1} and 0.2 g catalyst; the effect of pressure on the ammonia synthesis rate (*inset*). **b** The catalytic activities for ammonia synthesis over various 4 wt% Ru-loaded catalysts under the conditions: 598 K, 3 MPa, 5000 h^{-1} and 0.2 g catalyst

nearly inactive. Compared with the acid γ-Al_2O_3 support, the basic supports MgO, CeO_2 and g-C_3N_4 are prone to enhance the electron density of Ru nanoparticles, which could be easier to activate N_2 molecule. The ammonia synthesis activity of Ru/γ-Al_2O_3 was, therefore, much lower than the catalysts Ru/MgO, Ru/CeO_2 and Ru-H/g-C_3N_4. Although the basicity of MgO is much stronger than CeO_2, the activity of Ru/MgO was lower. This may be because MgO is an insulator and hence the support to metal electron transfer may not be very effective. The g-C_3N_4 is a typical n-type semiconductor [31] similar to CeO_2. And the electron-donating nitrogen, graphitization and the rich-electron π-plane enriched the electron density and dispersion of Ru nanoparticles. Besides, the d-band center of Ru nanoparticles was shifted up by the strong interaction between the rich-electron π-plane and Ru nanoparticles. Therefore, the activation of N_2 molecule on the catalyst Ru-H/g-C_3N_4 was more effective.

4 Conclusions

Ruthenium nanoparticles have been uniformly dispersed on g-C_3N_4 with electron-donating nitrogen and graphitic structure. Different pretreatment atmospheres significantly affected the interaction between Ru nanoparticles and the graphitic carbon nitride. The strong interaction leads not only to well-dispersed Ru particles with a mean size of 3.2 nm but also to the upshift of the Ru d-band center relative to the Fermi energy. Such upshift of d-band center gives rise to the easier activation of N_2 molecule.

Acknowledgments This research was financially supported by National Natural Science Foundation of China (Grant No. 21403257).

References

1. Dahl S, Törnqvist E, Chorkendorff I (2000) J Catal 192:381
2. Jacobsen CJH, Dahl S, Törnqvist PL, Törnqvist E, Jensen L, Topsøe H, Prip DV, Møenshaug PB, Chorkendorff I (2000) J Mol Catal A Chem 163:19
3. Kitano M, Inoue Y, Yamazaki Y, Hayashi F, Kanbara S, Matsuishi S, Yokoyama T, Kim SW, Hara M, Hosono H (2012) Nat Chem 4:934
4. Liang C, Li Z, Qiu J, Li C (2002) J Catal 211:278
5. Guo S, Pan X, Gao H, Yang Z, Zhao J, Bao X (2010) Chem Eur J 16:5379
6. Murata S, Aika KI (1992) J Catal 136:110
7. Gao WJ, Gao SJ, Zhang HB, Pan XL, Bao XH (2011) Chin J Catal 32:1418
8. Kitano M, Kanbara S, Inoue Y, Kuganathan N, Sushko PV, Yokoyama T, Hara M, Hosono H (2015) Nat Commun 6:6731
9. Lu Y, Li J, Tada T, Toda Y, Ueda S, Yokoyama T, Kitano M, Hosono H (2016) J Am Chem Soc 138:3970
10. Zhu J, Xiao P, Li H, Carabineiro SAC (2014) ACS Appl Mater Inter 6:16449
11. Wang Z, Wei J, Liu G, Zhou Y, Han K, Ye H (2015) Catal Sci Technol 5:3926
12. Wang Y, Yao J, Li H, Su D, Antonietti M (2011) J Am Chem Soc 133:2362
13. Gong Y, Zhang P, Xu X, Li Y, Li H, Wang Y (2013) J Catal 297:272
14. Li XH, Antonietti M (2013) Chem Soc Rev 42:6593
15. Liu X, Yao KX, Meng C, Han Y (2012) Dalton Trans 41:1289
16. Hammer B, Nørskov JK (1995) Nature 376:238
17. Xiao J, Pan X, Guo S, Ren P, Bao X (2015) J Am Chem Soc 137:477
18. Ruban A, Hammer B, Stoltze P, Skriver HL, Nørskov JK, J Mol Catal A Chem 115:pp 421
19. Lin BY, Wei KM, Ni J, Lin JX (2013) ChemCatChem 5:1941
20. Dong GH, Ho WK, Wang C (2015) J Mater Chem A 3:23435
21. Fernández C, Sassoye C, Debecker DP, Sanchez C, Ruiz P (2014) Appl Catal A 474:194
22. Lin BY, Qi YC, Guo YJ, Lin JX, Ni J (2015) Catal Sci Technol 5:2829
23. Zhou Z, Wang J, Yu J, Shen Y, Li Y, Liu A, Liu S, Zhang Y (2015) J Am Chem Soc 137:2179
24. Tenney SA, He W, Ratliff JS, Mullins DR, Chen DA (2011) Top Catal 54:42
25. Ma Z W, Xiong XM, Song CL, Hu B, Zhang WQ (2016) RSC Adv 6:51106
26. Prieto MJ, Carbonio EA, Fatayer S, Landers R, Siervo A (2014) Phys Chem Chem Phys 16:13329
27. Xu Y, Greeley J, Mavrikakis M (2005) J Am Chem Soc 127:12823
28. Yan SC, Li ZS, Zou ZG (2009) Langmuir 25:10397
29. Bojdys MJ, Müller JO, Antonietti M, Thomas A (2008) Chem Eur J 14:8177
30. Khabashesku VN, Zimmerman JL, Margrave JL (2000) Chem Mater 12:3264
31. Xu M, Han L, Dong S (2013) ACS Appl Mater Inter 5:12533